THE JOURNAL OF PHYSICAL CHEMISTRY B

Article

pubs.acs.org/JPCB

Local Unfolding and Aggregation Mechanisms of SOD1: A Monte Carlo Exploration

Anna Bille,[†] Sigurdur Æ. Jónsson,[†] Mikael Akke,[‡] and Anders Irbäck*[,†]

[†]Computational Biology and Biological Physics, Department of Astronomy and Theoretical Physics, Lund University, Sölvegatan 14A, SE-223 62 Lund, Sweden

[‡]Department of Biophysical Chemistry, Center for Molecular Protein Science, Lund University, P.O. Box 124, SE-22100 Lund, Sweden

Supporting Information

ABSTRACT: Copper, zinc superoxide dismutase 1 (SOD1) is a ubiquitous homodimeric enzyme, whose misfolding and aggregation play a potentially key role in the neurodegenerative disease amyotrophic lateral sclerosis (ALS). SOD1 aggregation is thought to be preceded by dimer dissociation and metal loss, but the mechanisms by which the metal-free monomer aggregates remain incompletely understood. Here we use implicit solvent all-atom Monte Carlo (MC) methods to investigate the local unfolding dynamics of the β-barrel-forming SOD1 monomer. Although event-to-event variations are large, on average, we find clear differences in dynamics among the eight strands forming the β-barrel. Most dynamic is the eighth strand, β8, which is located in the dimer interface of native SOD1. For the four strands in or near the dimer interface (β1, β2, β7, and β8), we perform aggregation simulations to assess the propensity of these chain segments to self-associate. We find that β1 and β2 readily self-associate to form intermolecular parallel β-sheets, whereas β8 shows a very low aggregation propensity.

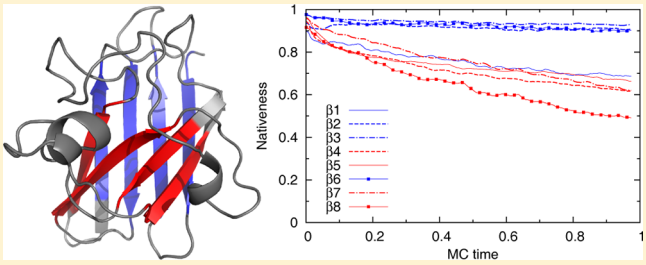

1. INTRODUCTION

The molecular mechanisms of the fatal motor neuron disease amyotrophic lateral sclerosis (ALS) are currently the subject of intense research.[1−4] While the majority of ALS cases (90−95%) are sporadic without known genetic link, mutations causing familial ALS have been identified in several molecules. About 20% of all familial ALS cases are linked to a set of more than 150 different mutations in the free-radical scavenging SOD1 enzyme.[5,6] To what extent misfolding and aggregation of wild-type SOD1 play a role in sporadic ALS is a debated question, but it is known that mutations can make SOD1 prone to misfold and aggregate. Further, some studies with conformation-specific antibodies,[7,8] but not all,[9] have found aberrant SOD1 in motor neurons in patients with sporadic ALS.

Many proteins linked to misfolding diseases are unstructured, such as the Alzheimer's amyloid β-peptide. SOD1 is, by contrast, very stable in its homodimeric native state. Each chain forms an eight-stranded immunoglobulin-like β-barrel that contains one intramolecular disulfide bond and binds one zinc and one copper ion. Two of the loops connecting the eight strands are long and functionally important. One is loop VII (residues 121−142), known as the electrostatic loop, which provides guidance of the superoxide substrate toward the catalytic copper site.[10] The other is the zinc-binding loop IV (residues 49−83). The zinc site is important for the structure and function of the active copper site.[11] The intramolecular disulfide bond connects Cys-57 in the zinc-binding loop to Cys-146 in the β8 strand. Another cysteine, Cys-111, has been found to be glutathionylized in human tissue,[12] a modification with a destabilizing effect on the dimer.[13] Dimer dissociation and metal loss are thought to precede aggregation.[14−16]

SOD1 can be made to form amyloid fibrils in vitro,[17,18] but amyloid structures have not been linked to ALS; the character of potentially ALS-linked aggregates remains unknown. Especially in view of this uncertainty, the initial events on the aggregation pathway are of particular interest. Factors that could drive SOD1 aggregation include flexibility of the electrostatic and zinc-binding loops in the absence of metal ions,[19] intermolecular Cys-6,Cys-111 cross-linking,[20,21] mutation-mediated reduction of net charge,[22] and oxidation-induced misfolding.[23] In addition, it is known that the metal-free disulfide-reduced monomer is only marginally stable at physiological temperature,[24,25] which hints at partial or complete unfolding of the β-barrel core as a possible aggregation-triggering mechanism. The extent of unfolding required to initiate aggregation is, however, unclear. Partially unfolded and potentially aggregation-prone states have been identified,[26,27] but it could be that the precursor for aggregation is a globally unfolded state.[28]

Received: May 6, 2013
Revised: July 11, 2013
Published: July 11, 2013

   dx.doi.org/10.1021/jp404500b | J. Phys. Chem. B 2013, 117, 9194−9202

Further insights into the structural properties of SOD1 have come from computational studies. Several groups used molecular dynamics simulations to examine the structure and dynamics of the native state.[29−35] These simulations are, for a protein of this size, limited to short time scales. Large-scale structural properties of SOD1 have been studied by Ding, Dokholyan, and co-workers, by using the computationally efficient discrete molecular dynamics method.[36−38] Another very recent approach is that of Das and Plotkin,[39,40] where a local measure of force resistance is computed and analyzed. The resulting "mechanical fingerprint" of SOD1 provided insight into the internal stress of the native structure. A bioinformatics-based study of conformational fluctuations in native SOD1 has also been reported.[41]

In this article, we present an implicit solvent all-atom MC study of SOD1 in two parts. First, we study the local unfolding dynamics of the monomer. Our main focus is on the wild-type (WT) protein in metal-free disulfide-reduced (apo-red) form. For comparison, we also study the apo-red C6A/F50E/G51E/C111A and I149T mutants and the metal-bound disulfide-oxidized (holo-ox) WT protein. These calculations aim at identifying dynamic parts of the β-barrel core, whose unfolding could initiate aggregation. Our results point at β8 as the most dynamic β-barrel strand in the apo-red WT monomer.

Having seen this, in the second part of our study, we perform aggregation simulations for β8 and three strands located near β8 in the native β-barrel, namely β1, β2, and β7. The aggregation properties of these chain segments have, as far as we know, not been simulated before. We find that β1 and especially β2 have a strong tendency to form parallel intermolecular β-structure, whereas β8 shows a very low self-association propensity.

2. METHODS

2.1. Model. Our simulations are based on an implicit solvent all-atom representation with torsional degrees of freedom combined with an effective potential for proteins in solution. The potential, described in detail elsewhere,[42] is composed of four terms, $E = E_{loc} + E_{ev} + E_{hb} + E_{sc}$. In brief, the first term, E_{loc}, contains local interactions between atoms separated by only a few covalent bonds, whereas the other three terms are nonlocal in character: E_{ev} represents excluded-volume effects, E_{hb} is a hydrogen-bond potential, and E_{sc} describes residue-specific interactions, based on hydrophobicity and charge, between pairs of side chains. The potential was parametrized through folding thermodynamics studies for a diverse set of peptides and small proteins.[42] The above approach has been used for a range of protein simulation studies, including investigations of thermal and mechanical unfolding[43,44] and of aggregation.[45−47]

We study both apo-red and holo-ox variants of the SOD1 monomer. In the holo-ox simulations, we use harmonic restraints between pairs of atoms to model the Cys-57,Cys-146 disulfide bond and the binding of the two metal ions. Equilibrium distances for the harmonic potentials are taken from a crystal structure (PDB ID 2V0A[34]). The disulfide bond is described using a set of four distance restraints involving the S and C^β atoms of the two cysteine residues. The binding of a copper or a zinc ion is modeled using 12 distance restraints among the coordinating atoms.

2.2. MC Details. We investigate the local unfolding properties of the SOD1 monomer using MC dynamics. MC is a crude approximation to the real dynamics over short time scales, but we expect MC-based simulations to capture the major free-energy minima and barriers encountered by a protein upon unfolding, provided that only small trial moves are used.[48,49] Our unfolding simulations are carried out using two MC updates: rotations of single side-chain angles and coordinated "biased Gaussian steps" (BGS) for backbone angles.[50] BGS is a semilocal backbone update that turns up to eight consecutive torsion angles in a manner that keeps the ends of the updated segment approximately fixed. The ratio of backbone to side-chain updates is 1:1.

We examine the aggregation propensity of SOD1 fragments by MC-based equilibrium simulations of systems of three chains, enclosed in a periodic box of size $(40\ \text{Å})^3$. For each peptide, we use acetyl and amide as N- and C-terminal capping groups. Starting from random initial conditions, we simulate a set of eight temperatures, geometrically distributed between 273 and 400 K, by the replica exchange method.[51] The conformational moves are of five types: (i) pivot rotations of individual backbone angles, (ii) BGS backbone updates, (iii) rotations of individual side-chain angles, (iv) rigid-body translations of whole chains, and (v) rigid-body rotations of whole chains. The relative frequencies of the updates (i)−(v) are 25%, 12%, 47%, 8%, and 8%, respectively. All our simulations are carried out using the program PROFASI.[52]

2.3. Initial Conformations. The conformations serving as starting points for our different monomer simulations were derived from a crystal structure (PDB ID 2V0A) by a simulated annealing-like procedure. The cost function was a linear combination of the energy E and an rmsd-based term penalizing deviations from the crystal structure. The relative weight of the energy term was gradually increased during the course of the runs. Finally, a structure with both low E and low rmsd was selected. The holo-ox WT model structure was generated including terms representing metal binding and the disulfide bond, which were omitted in the apo-red WT case. The apo-red C6A/F50E/G51E/C111A and I149T model structures were created by manual mutations of the derived apo-red WT structure, followed by brief relaxations of side-chain degrees of freedom. The rmsd from the crystal structure (calculated over backbone and C^β atoms) was ∼1 Å for the model structures.

To assess the robustness of our findings with respect to the initial conditions, we repeated the simulations described below for both apo-red WT and holo-ox WT starting from different initial conformations, derived using other crystal structures (PDB ID 1HL4 for apo-red WT and PDB ID 1HL5 for holo-ox WT[53]). The changes in initial structure had only marginal effects on the results (see Supporting Information, Figures S1 and S2) and did not affect any of our conclusions.

2.4. Analysis. We monitor the unfolding of the monomer using a local measure of nativeness, defined in terms of C^α−C^α distances, r_{ij}.[54] Let s_{ij} denote the native C^α−C^α distance between residues i and j, and let, given i, A_i be the set of residues j for which $s_{ij} < 6$ Å and $|i-j| > 2$. The nativeness Q_i of residue i is a number between 0 and 1, calculated as

$$Q_i = \frac{1}{N_i} \sum_{j \in A_i} e^{-(r_{ij}-s_{ij})^2/\xi^2} \quad (1)$$

where N_i is the size of the set A_i and ξ is a parameter set to 3 Å.

Secondary structure is classified using the program STRIDE.[55] The β-structure content, B, is computed as the fraction of residues that are in the class extended.

dx.doi.org/10.1021/jp404500b | J. Phys. Chem. B 2013, 117, 9194−9202

Throughout the paper, error bars and shaded areas represent one standard error of the mean.

3. LOCAL UNFOLDING OF THE MONOMER

The native structure of the SOD1 monomer is illustrated in Figure 1. The eight-stranded β-barrel core is not perfectly

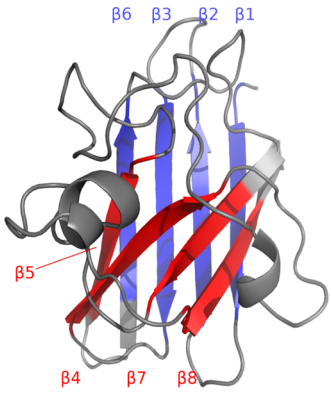

Figure 1. Schematic illustration of the native structure of the SOD1 monomer. The first β-sheet (strands β1, β2, β3, and β6) is indicated in blue and the second (β5, β4, β7, and β8) in red. The structure is our model approximation for the apo-red WT monomer, derived from a crystal structure (PDB ID 2V0A) by simulated annealing. Drawn with PyMOL.[56]

cylindrical, but can be viewed as composed of two four-stranded β-sheets, which are colored blue and red, respectively. The first sheet consists of the strands β1, β2, β3, and β6, and the second one comprises β5, β4, β7, and β8. The definition of the strands can be found in Table 1. The two strand pairs

Table 1. Strand Segments in the β-Barrel Core of the SOD1 Monomer

strand	residues	sequence
β1	2−9	TKAVCVLK
β2	15−22	QGIINFEQ
β3	29−36	VKVWGSIK
β4	41−48	GLHGFHVH
β5	83−89	DLGNVTA
β6	95−101	ADVSIED
β7	116−120	TLVVH
β8	143−148	RLACGV

connecting the β-sheets into a barrel are β1,β8 and β5,β6. The β1,β8 pair is located in the dimer interface of native SOD1. The β5,β6 pair is protected by the electrostatic and zinc-binding loops, which become more dynamic upon metal loss. Hence, both pairs of edge strands are more exposed in the apo monomer than they are in the holo dimer.

We study four variants of the SOD1 monomer: apo-red WT, holo-ox WT, and the apo-red I149T and C6A/F50E/G51E/C111A mutants. A figure showing the positions of the mutations in the native structure can be found in Supporting Information (Figure S3). For each variant, we generate a set of 64 independent MC trajectories at a simulation temperature of 320 K, starting from native initial conditions. To characterize the structure and stability of the β-barrel, we monitor the MC time evolution of the β-structure content B and the average nativeness Q (see eq 1) for the eight strand segments.

3.1. Apo-red WT and Pseudo-WT. The experimental melting temperature of apo-red WT is 315−320 K,[24,25] which is close to our simulation temperature (320 K). Consistent with this, we observe a partial unfolding of the β-barrel with MC time (Figure 2). The unfolding does not occur in a uniform manner; some strands are more rigid than others. One clear trend is for strands in the first β-sheet (blue curves) to be more stable than those of the second β-sheet (red curves). This conclusion supports experimental NMR data on transient perturbations of different apo-red as well as apo-ox variants.[27] Particularly stable are the two central strands of the first β-sheet, β2 and β3. Both the β-structure content B and the nativeness Q stay high throughout the whole simulations for these two segments. Most dynamic is β8, an edge strand in the second β-sheet. The remaining five strands are all grouped between these extremes. The one exception is β6, which is lower in B but similar in Q compared to β2 and β3. Within the stable first β-sheet, one strand is below the others in terms of Q, namely β1. This does not imply that β1 has a tendency to detach from the rest of this β-sheet; the lower Q of β1 largely just reflects the loss of its neighbor β8.

It is important to note that Figure 2 shows averages over many independent runs. Inspection shows that the run-to-run variations are large. For instance, although β8 is least stable among the strands, it does not unfold first in every single run. Figure 3 shows the MC time evolution in three individual runs, to illustrate the stochastic nature of the dynamics. Snapshots from these runs can be found in the Supporting Information (Figures S4, S5, and S6). The first example (Figure 3a,b) is a

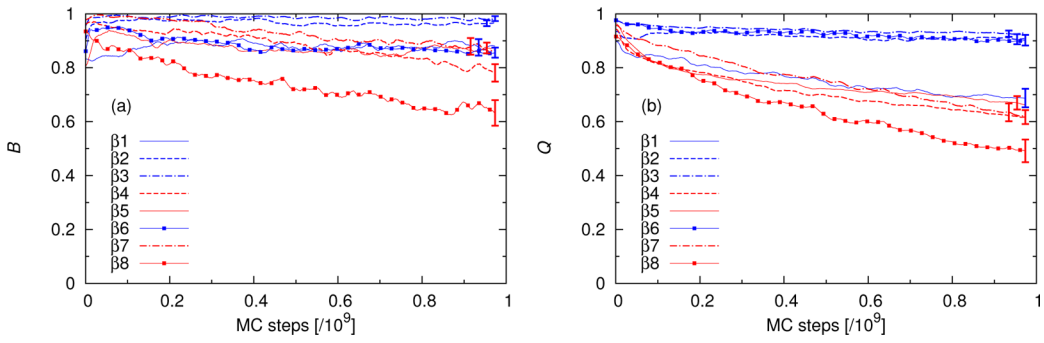

Figure 2. MC time evolution of ensemble averages in unfolding simulations of the apo-red WT monomer. The stability of the strands β1-β8 is assessed using (a) the β-structure content B and (b) the nativeness Q. The curves are averages over 64 independent runs and smoothed to improve readability. Error bars show the statistical uncertainties at the end of the simulated time period, where they are largest. The color coding is as in Figure 1. The first β-sheet (blue curves) is more stable than the second (red curves).

dx.doi.org/10.1021/jp404500b | J. Phys. Chem. B 2013, 117, 9194−9202

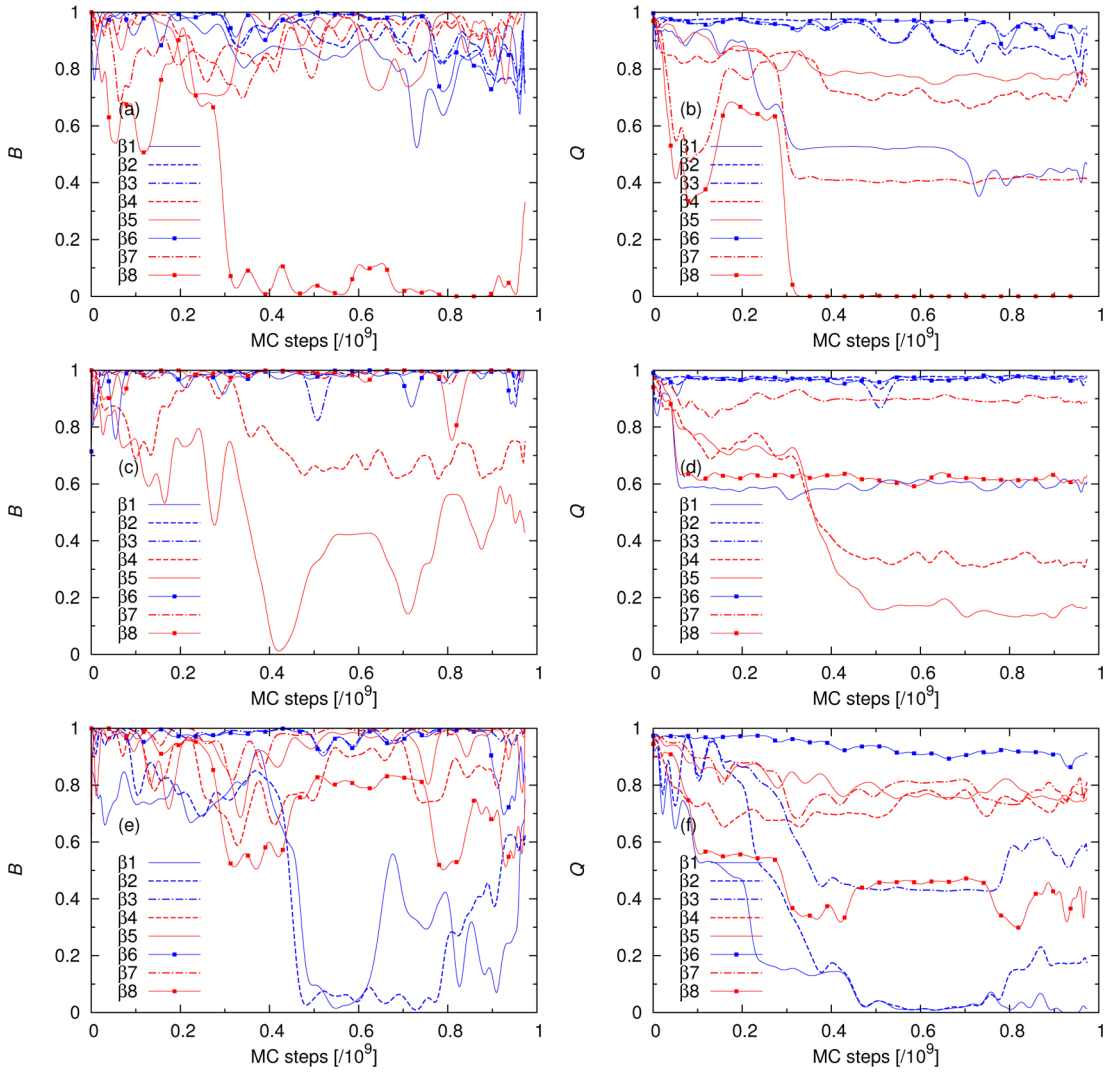

Figure 3. Examples of individual MC trajectories for the apo-red WT monomer. Three individual runs are shown out of the 64 runs used to form the averages shown in Figure 2. The strands undergoing the largest conformational changes are β8 in the first run (a,b), β5 in the second run (c,d), and β1 and β2 in the third run (e,f).

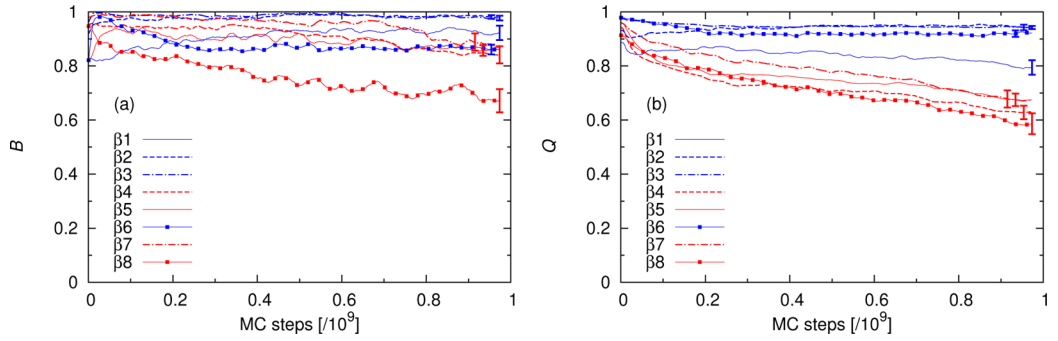

Figure 4. MC time evolution of ensemble averages for the apo-red pseudo-WT (C6A/F50E/G51E/C111A) monomer. The layout follows that of Figure 2. Error bars show the statistical uncertainties at the end of the simulated time period, where they are largest. The results are very similar to those for apo-red WT (Figure 2), except that β1 and β8 have higher Q for the pseudo-WT protein.

run in which the barrel loses one of its strands, namely β8. The loss of β8 is signaled by a sudden and simultaneous drop in both *B* and Q to very low values. The rest of the β-barrel remains intact throughout the whole simulation, despite the loss of β8. The opening of the barrel caused by the loss of β8 leads to fewer native contacts for the neighboring strands β1 and β7. However, β1 and β7 remain attached to their other neighbors (β2 and β4, respectively), and therefore their Q values do not go below ~0.4. The behavior seen in the second example (Figure 3c,d) does not correspond to a simple loss of a single strand, but is more complex. Very early in this run, there is a drop in Q for β1 and β8, reflecting a partial opening of the

dx.doi.org/10.1021/jp404500b | J. Phys. Chem. B 2013, 117, 9194−9202

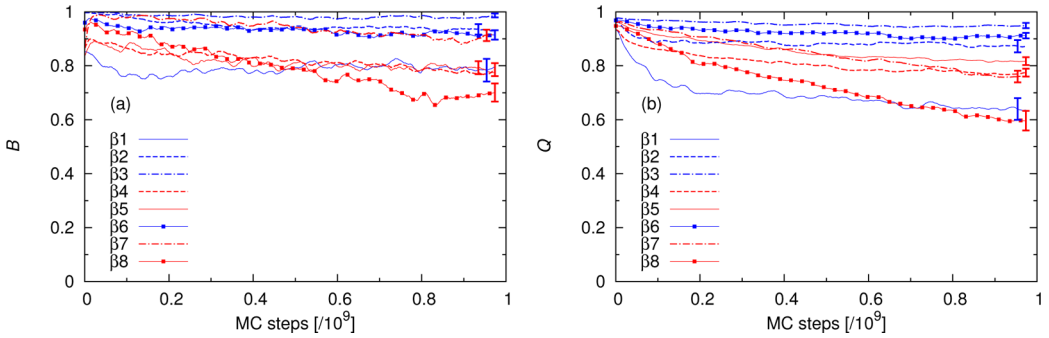

Figure 5. MC time evolution of ensemble averages for the holo-ox WT monomer. The layout follows that of Figure 2. Error bars show the statistical uncertainties at the end of the simulated time period, where they are largest. The second β-sheet (red curves) is more stable than it is in the apo-red WT monomer (Figure 2).

barrel between these strands. Later in the run, a reorganization occurs that involves the other pair of edge strands, namely $\beta5$ and $\beta6$. However, the coupling between $\beta5$ and $\beta6$ gets stronger rather than weaker, which occurs at the expense of contacts between $\beta5$ and $\beta4$. As a result, the barrel opens up between $\beta5$ and $\beta4$. During this reorganization, the β-structure content of $\beta5$ temporarily drops to zero. The third and final example (Figure 3e,f) is a run in which the barrel loses two strands at the same time, namely $\beta1$ and $\beta2$. Both B and Q decrease to very low values for $\beta1$ and $\beta2$, and there is a significant drop in Q for the adjacent strands $\beta3$ and $\beta8$ as well. Toward the end of the run, $\beta1$ and $\beta2$ form β-structure again, but it is mainly non-native (Q remains low). Note that the averages over all trajectories (Figure 2) show that $\beta2$ is very stable in the model. This third example thus demonstrates that even very stable strands may occasionally unfold completely.

A pseudo-WT SOD1 variant useful for in vitro studies of the structure and dynamics of the monomer is C6A/F50E/G51E/C111A.[26] Here, mutating the two cysteines yields highly reversible folding/unfolding, whereas the introduction of the two charged glutamic acid residues suppresses dimerization. We simulate the apo-red C6A/F50E/G51E/C111A variant using the same setup as for apo-red WT. The resulting pseudo-WT trajectories (Figure 4) are very similar to those above for WT (Figure 2). The only notable difference is an increase in Q in the pseudo-WT case for the neighboring edge strands $\beta1$ and $\beta8$. In the mutated protein, $\beta8$ is only marginally more dynamic compared to the other strands of the second β-sheet.

3.2. Holo-ox WT. To examine how metal binding and disulfide bond formation affect the dynamics of the SOD1 monomer, we repeated the same simulation procedure for holo-ox WT at an unchanged simulation temperature (320 K). In the holo-ox WT simulations, we also observe a slight drift in β-structure content and nativeness with MC time (Figure 5). Given the high stability of the holo-ox WT dimer, which has a melting temperature of ~365 K,[57] the present results on the holo-ox WT monomer might suggest that the simulations underestimate the overall stability of this variant. Nevertheless, compared to apo-red WT, we observe a marked increase in stability for the holo-ox WT monomer, with the greatest difference between the two variants being observed for the second β-sheet. The two most dynamic strands of the holo-ox WT monomer, in terms of Q, are $\beta1$ and $\beta8$, the two edge strands in the dimer interface of native SOD1.

To get information on the loop regions as well, we also do a global analysis of Q_i (eq 1) over the whole sequence. For residues without any contact in the native state, Q_i is undefined ($N_i = 0$). For all other residues, we determine an average Q_i, $\bar{Q}_i$, using the last 10% of every run. The resulting $\bar{Q}_i$ profiles show that metal binding and disulfide bond formation have a strong impact on the electrostatic and zinc-binding loops (Figure 6). These loops are partially structured for holo-ox WT,

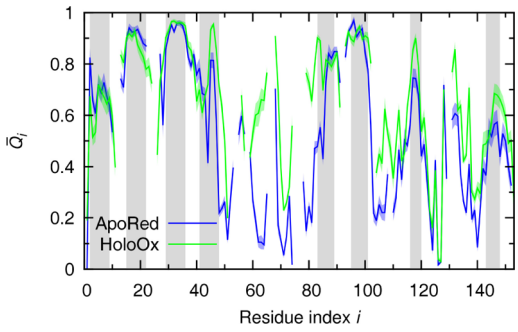

Figure 6. Nativeness, $\bar{Q}_i$, plotted against residue number, i, for holo-ox WT (green) and apo-red WT (blue), as obtained by averaging over the last 10% of all the 64 unfolding runs. Breaks in the curves occur because Q_i (eq 1) is undefined for residues lacking native contacts. The shaded bands surrounding the curves indicate statistical uncertainties. Vertical gray bars indicate the strand regions $\beta1-\beta8$.

but very dynamic for apo-red WT, in keeping with previous NMR results.[27] Likewise, the second β-sheet has higher $\bar{Q}_i$ values for holo-ox WT than for apo-red WT. The first β-sheet has, by contrast, very similar $\bar{Q}_i$ values for both variants.

3.3. Apo-red I149T. Having found $\beta8$ to be the most dynamic strand of the apo-red WT monomer, we finally study the effects of a single-point mutation, I149T, that is located near this strand and linked to familial ALS. A study of the protease resistance of agitation-induced fibrils found this mutation to alter the fibril core architecture.[58]

The dynamics of the β-barrel core in our apo-red I149T simulations (at 320 K) is illustrated in Figure 7. Comparison to the apo-red WT results (Figure 2) shows that this mutation has a destabilizing effect on the entire second β-sheet (red curves). While significantly weakening this β-sheet, the mutation has only limited effects on the first β-sheet; in fact, the $\beta2$, $\beta3$, and $\beta6$ strands are all left essentially unaffected by the mutation. The difference in stability between the two β-sheets is thus enhanced by the I149T mutation. The I149T mutation leads to a 5-fold reduction in Q for $\beta8$, which remains the most dynamic strand after the mutation. This result is largely in agreement with experimental studies on the kinetic and equilibrium unfolding properties of other I149 mutants.[26] Within the

dx.doi.org/10.1021/jp404500b | J. Phys. Chem. B 2013, 117, 9194−9202

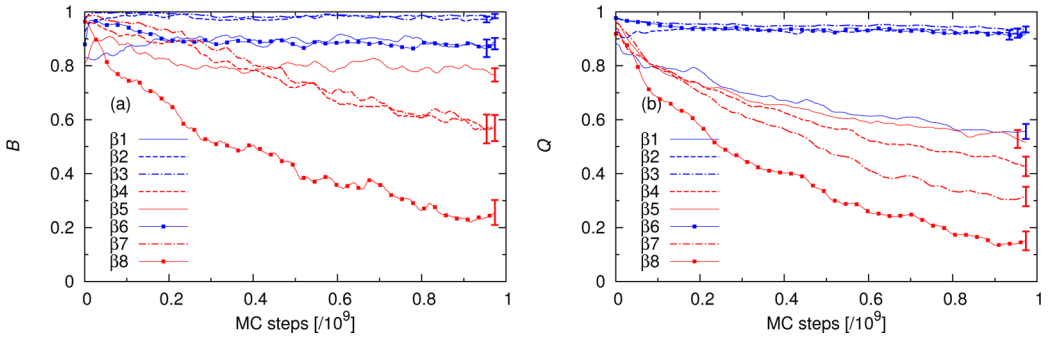

Figure 7. MC time evolution of ensemble averages for the apo-red I149T monomer. The layout follows that of Figure 2. Error bars show the statistical uncertainties at the end of the simulated time period, where they are largest. The second β-sheet (red curves) is more dynamic than it is in the apo-red WT monomer (Figure 2).

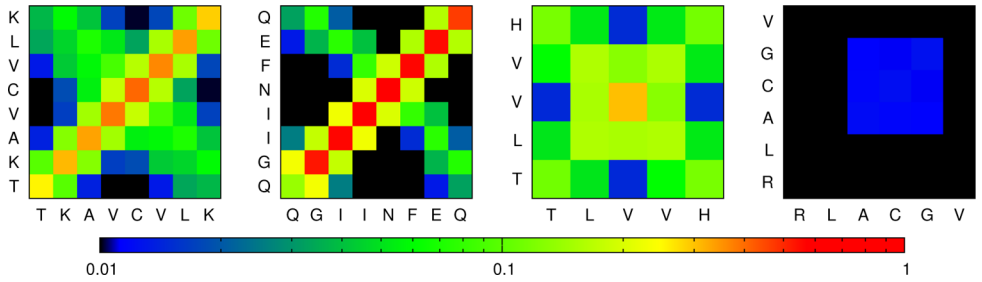

Figure 8. Probability maps of interchain residue contact formation for (from left to right) β1, β2, β7, and β8, as obtained from simulations with three chains at 273 K. Two residues are in contact if the C^{α}–C^{α} distance is <6 Å. β1 and β2 show a high propensity for forming parallel intermolecular β-structure, as reflected by high probabilities along the main diagonal of the contact map. β7 has a significant but lower aggregation propensity, and no clear preference for either parallel or antiparallel β-structure. β8 shows a low aggregation propensity.

second β-sheet, the stability of the strands increases steadily with distance from β8 (β8 < β7 < β4 < β5). A likely unfolding pattern therefore is that the β-barrel core opens up through the loss of β8, followed by the unfolding of adjacent strands in the second β-sheet.

4. AGGREGATION PROPENSITY OF β1, β2, β7, AND β8

The dynamic nature of β8 seen above hints that this and the neighboring β-barrel strands could play a key role in aggregation. To assess their relative propensities to self-associate, we performed aggregation simulations with three chains for each of the β1, β2, β7, and β8 segments, using a temperature of 273 K and starting from random initial conditions. The setup was the same as in previous studies of related systems.[45−47] We analyze the aggregation properties by computing probability maps of interchain residue contact formation (Figure 8). A residue pair is said to be in contact if their C^{α} atoms are within 6 Å.

The calculated contact maps reveal clear differences in aggregation propensity among these four segments (Figure 8). To quantify the aggregation propensity, we calculate the average number of interchain contacts divided by the number of amino acids in the system, n_c. The most aggregation prone segment is β2, with n_c = 0.95, whereas β8 shows a very low aggregation propensity, with n_c = 0.05. The corresponding values for β1 and β7 are n_c = 0.76 and n_c = 0.49, respectively. Both β2 and β1 show a strong preference for parallel over antiparallel β-structure; the highest values in their contact maps are found along the main diagonal. The β7 segment shows, by contrast, no clear preference for either parallel or antiparallel strand organization.

The relative aggregation propensities of these four peptides have, as far as we know, not been studied experimentally. We therefore compare our findings to results generated by the aggregation predictor tool PASTA.[59] Given an input sequence, PASTA minimizes a pair energy over different strand alignments. The minimum energies found for the β2, β7, β1, and β8 sequences are −5.38, −5.37, −4.76, and −2.04, respectively, where a value below −4 is indicative of a propensity for fibril formation.[59] Overall, these values match very well with our simulation results. In both cases, β2 is the most aggregation prone segment, while β8 has little or no tendency to aggregate. A difference compared to the PASTA results is in the relative aggregation propensity of β1 and β7. The β7 segment is less aggregation prone in the simulations, compared to what one would expect based on the PASTA predictions.

We also performed aggregation simulations for the other four strands (β3, β4, β5, β6). Contact maps and a list of simulated n_c values and PASTA energies for all eight strands can be found in the Supporting Information (Figure S7 and Table S1).

5. DISCUSSION

By generating and analyzing large sets of MC-based trajectories, we have investigated the local unfolding dynamics of the SOD1 monomer. In our simulations, the β-barrel strands do not unfold in a well-defined order, but statistically some strands are more dynamic than others. One clear trend seen in the apo-red WT simulations is for the second β-sheet (β5, β4, β7, β8) to be much more dynamic than the first (β1, β2, β3, β6), which is in perfect agreement with NMR results on apo variants in the monomeric form[27,60] as well as with computational analysis.[36] For comparison, using the same setup, we also simulated the

dx.doi.org/10.1021/jp404500b | J. Phys. Chem. B 2013, 117, 9194−9202

holo-ox WT and apo-red I149T variants. We find that metal binding and disulfide bond formation reduce the differences in mobility within the β-barrel by having a stabilizing effect on the second β-sheet, which also matches very well with experiments.[60] By contrast, we find the I149T mutation to destabilize the second β-sheet even further, while having only marginal effects on the first β-sheet. This result is in line with kinetic folding−unfolding experiments[26] and discrete molecular dynamics simulations.[38] The electrostatic and zinc-binding loops are partially structured in the holo-ox WT simulations, but highly dynamic for the two apo-red variants. Again, a number of NMR studies have indicated that metal binding diminishes the conformational fluctuations of the loops.[27,60] The simulations are thus in good overall agreement with experimental results.

At a more detailed level, in the β-barrel core of the apo-red WT monomer, we find β8 to be the most dynamic strand. This finding may be compared with experimental results on the apo-red monomer obtained by ϕ-value analysis[26] and NMR methods[27] using the pseudo-WT C6A/F50E/G51E/C111A variant. These experiments support the conclusion that β8 is dynamic. However, relative to the other strands of the second β-sheet, β8 seems to be even more dynamic in the simulations than it is in the experiments. Therefore, we also performed the corresponding simulations for the pseudo-WT variant (C6A/F50E/G51E/C111A). Our results for this variant (Figure 4) are very similar to those for WT (Figure 2), and suggest, in particular, that the mutant does not artificially increase the dynamics of the protein. In fact, in our simulations, the only notable difference between these two variants is that β1 and β8 display somewhat reduced dynamic fluctuations (higher Q) in the pseudo-WT protein. This difference may explain why β8 stands out as more dynamic than the other strands in our WT simulations, whereas this property was not seen in the experiments.

Our identification of β8 as highly dynamic in the apo-red WT monomer matches well with the very recent computational analysis of Das and Plotkin.[40] These authors found that the order induced by structuring β8 causes frustration and strain in the protein. In particular, they found that a truncation mutant lacking β8, G127X, exhibits reduced dynamic fluctuations compared to the full-length protein.[40]

Our aggregation simulations for the β1, β2, β7, and β8 segments suggest that the self-association propensity varies widely, from very low for β8 to high for β1 and especially β2. The observation of a high aggregation propensity for β2 is, as mentioned earlier, in perfect agreement with predictions generated by the PASTA server.[59] Another aggregation prediction program, WALTZ,[61] also points at this SOD1 segment as particularly aggregation prone.[62] We find that the aggregation propensity is high for β1 as well; both β1 and β2 readily form parallel intermolecular β-structure in the simulations. This finding hints at a potentially important role in aggregation for β1, which is located next to the dynamic β8 strand in the β-barrel. If β1 unfolds from the core and engages in intermolecular β-interactions, then β2 can also form such structures, essentially zipping up the entire β1−β2 stretch via intermolecular contacts. Mutant variants that affect the stability of the native β1−β2 interactions, such as A4V,[27] might play an important role in this respect.

6. CONCLUSION

Using implicit solvent all-atom MC simulations, we have examined the local unfolding dynamics of the SOD1 monomer and the aggregation properties of four strand segments from its β-barrel core. Our main findings are as follows. (i) In the apo-red WT monomer, the second β-sheet is more dynamic than the first, and most dynamic among the individual strands is β8. The dynamic fluctuations of both β8 and β1 are reduced in the pseudo-WT C6A/F50E/G51E/C111A variant, which otherwise shows unfolding properties very similar to those of WT. (ii) The β1 and β2 segments readily self-associate to form parallel intermolecular β-sheets, whereas the aggregation propensity of β8 is very low. These findings suggest potential mechanisms for SOD1 misfolding and aggregation.

■ ASSOCIATED CONTENT

Supporting Information

Run-time evolution in simulations with alternative initial structures. Folded structure with mutations indicated. Examples of partially unfolded structures. Results from aggregation simulations and PASTA energies for all the strand segments β1−β8. This material is available free of charge via the Internet at http://pubs.acs.org.

■ AUTHOR INFORMATION

Corresponding Author

*E-mail: anders@thep.lu.se.

Notes

The authors declare no competing financial interest.

■ ACKNOWLEDGMENTS

This work was supported in part by the FLÄK research school, Lund University, and the Swedish Research Council (2010-2478). The simulations were performed on resources provided by the Swedish National Infrastructure for Computing (SNIC) at LUNARC, Lund University.

■ REFERENCES

(1) Valentine, J. S.; Doucette, P. A.; Potter, S. Z. Copper-Zinc Superoxide Dismutase and Amyotrophic Lateral Sclerosis. *Annu. Rev. Biochem.* **2005**, *74*, 563−593.

(2) Chiti, F.; Dobson, C. M. Amyloid Formation by Globular Proteins under Native Conditions. *Nat. Chem. Biol.* **2009**, *5*, 15−22.

(3) Robberecht, W.; Philips, T. The Changing Scene of Amyotrophic Lateral Sclerosis. *Nat. Rev. Neurosci.* **2013**, *14*, 248−264.

(4) Mulligan, V. K.; Chakrabartty, A. Protein Misfolding in the Late-Onset Neurodegenerative Diseases: Common Themes and the Unique Case of Amyotrophic Lateral Sclerosis. *Proteins* **2013**, DOI: 10.1002/prot.24285.

(5) Rosen, D. R.; et al. Mutations in Cu/Zn Superoxide Dismutase Gene are Associated with Familial Amyotrophic Lateral Sclerosis. *Nature* **1993**, *362*, 59−62.

(6) Cleveland, D. W.; Rothstein, J. D. From Charcot to Lou Gehrig: Deciphering Selective Motor Neuron Death in ALS. *Nat. Rev. Neurosci.* **2001**, *2*, 806−819.

(7) Bosco, D. A.; Morfini, G.; Karabacak, N. M.; Song, Y.; Gros-Louis, F.; Pasinelli, P.; Goolsby, H.; Fontaine, B. A.; Lemay, N.; McKenna-Yasek, D.; Frosch, M. P.; Agar, J. N.; Julien, J.-P.; Brady, S. T.; Brown, R. H. Wild-Type and Mutant SOD1 Share an Aberrant Conformation and a Common Pathogenic Pathway in ALS. *Nat. Neurosci.* **2010**, *13*, 1396−1403.

(8) Forsberg, K.; Jonsson, P. A.; Andersen, P. M.; Bergemalm, D.; Graffmo, K. S.; Hultdin, M.; Jacobsson, J.; Rosquist, R.; Marklund, S. L.; Brännström, T. Novel Antibodies Reveal Inclusions Containing

Non-Native SOD1 in Sporadic ALS Patients. *PLoS One* **2010**, *5*, e11552.
(9) Kerman, A.; Liu, H.-N.; Croul, S.; Bilbao, J.; Rogaeva, E.; Zinman, L.; Robertson, J.; Chakrabartty, A. Amyotrophic Lateral Sclerosis is a Non-Amyloid Disease in Which Extensive Misfolding of SOD1 is Unique to the Familial Form. *Acta Neuropathol.* **2010**, *119*, 335−344.
(10) Getzoff, E. D.; Cabelli, D. E.; Fisher, C. L.; Parge, H. E.; Viezzoli, M. S.; Banci, L.; Hallewell, R. A. Faster Superoxide Dismutase Mutants Designed by Enhancing Electrostatic Guidance. *Nature* **1992**, *358*, 347−351.
(11) Nordlund, A.; Leinartaite, L.; Saraboji, K.; Aisenbrey, C.; Gröbner, G.; Zetterström, P.; Danielsson, J.; Logan, D. T.; Oliveberg, M. Functional Features Cause Misfolding of the ALS-Provoking Enzyme SOD1. *Proc. Natl. Acad. Sci. U.S.A.* **2009**, *106*, 9667−9672.
(12) Wilcox, K. C.; Zhou, L.; Jordon, J. K.; Huang, Y.; Yu, Y.; Redler, R. L.; Chen, X.; Caplow, M.; Dokholyan, N. V. Modifications of Superoxide Dismutase (SOD1) in Human Erythrocytes: A Possible Role in Amyotrophic Lateral Sclerosis. *J. Biol. Chem.* **2009**, *284*, 13940−13947.
(13) Redler, R. L.; Wilcox, K. C.; Proctor, E. A.; Fee, L.; Caplow, M.; Dokholyan, N. V. Glutathionylation at Cys-111 Induces Dissociation of Wild Type and FALS Mutant SOD1 Dimers. *Biochemistry* **2011**, *50*, 7057−7066.
(14) Rakhit, R.; Crow, J. P.; Lepock, J. R.; Kondejewski, L. H.; Cashman, N. R.; Chakrabartty, A. Monomeric Cu,Zn-Superoxide Dismutase is a Common Misfolding Intermediate in the Oxidation Models of Sporadic and Familial Amyotrophic Lateral Sclerosis. *J. Biol. Chem.* **2004**, *279*, 15499−15504.
(15) Khare, S. D.; Caplow, M.; Dokholyan, N. V. The Rate and Equilibrium Constants for a Multistep Reaction Sequence for the Aggregation of Superoxide Dismutase in Amyotrophic Lateral Sclerosis. *Proc. Natl. Acad. Sci. U.S.A.* **2004**, *101*, 15094−15099.
(16) Doucette, P. A.; Whitson, L. J.; Cao, X.; Schirf, V.; Demeler, B.; Valentine, J. S.; Hansen, J. C.; Hart, P. J. Dissociation of Human Copper-Zinc Superoxide Dismutase Dimers Using Chaotrope and Reductant. Insights into the Molecular Basis for Dimer Stability. *J. Biol. Chem.* **2004**, *279*, 54558−54566.
(17) Chattopadhyay, M.; Durazo, A.; Sohn, S. H.; Strong, C. D.; Gralla, E. B.; Whitelegge, J. P.; Valentine, J. S. Initiation and Elongation in Fibrillation of ALS-Linked Superoxide Dismutase. *Proc. Natl. Acad. Sci. U.S.A.* **2008**, *105*, 18663−18668.
(18) Furukawa, Y.; Kaneko, K.; Yamanaka, K.; O'Halloran, T. V.; Nukina, N. Complete Loss of Post-Translational Modifications Triggers Fibrillar Aggregation of SOD1 in the Familial Form of Amyotrophic Lateral Sclerosis. *J. Biol. Chem.* **2008**, *283*, 24167−24176.
(19) Elam, J. S.; Taylor, A. B.; Strange, R.; Antonyuk, S.; Doucette, P. A.; Rodriguez, J. A.; Hasnain, S. S.; Hayward, L. J.; Valentine, J. S.; Yeates, T. O.; Hart, P. J. Amyloid-Like Filaments and Water-Filled Nanotubes Formed by SOD1 Mutant Proteins Linked to Familial ALS. *Nat. Struct. Biol.* **2003**, *10*, 461−467.
(20) Banci, L.; Bertini, I.; Durazo, A.; Girotto, S.; Gralla, E. B.; Martinelli, M.; Valentine, J. S.; Vieru, M.; Whitelegge, J. P. Metal-Free Superoxide Dismutase Forms Soluble Oligomers under Physiological Conditions: A Possible General Mechanism for Familial ALS. *Proc. Natl. Acad. Sci. U.S.A.* **2007**, *104*, 11263−11267.
(21) Niwa, J.; Yamada, S.; Ishigaki, S.; Sone, J.; Takahashi, M.; Katsuno, M.; Tanaka, F.; Doyu, M.; Sobue, G. Disulfide Bond Mediates Aggregation, Toxicity, and Ubiquitylation of Familial Amyotrophic Lateral Sclerosis-Linked Mutant SOD1. *J. Biol. Chem.* **2007**, *282*, 28087−28095.
(22) Sandelin, E.; Nordlund, A.; Andersen, P. M.; Marklund, S. S. L.; Oliveberg, M. Amyotrophic Lateral Sclerosis-Associated Copper/Zinc Superoxide Dismutase Mutations Preferentially Reduce the Repulsive Charge of the Proteins. *J. Biol. Chem.* **2007**, *282*, 21230−21236.
(23) Mulligan, V. K.; Kerman, A.; Laister, R. C.; Sharda, P. R.; Arslan, P. E.; Chakrabartty, A. Early Steps in Oxidation-Induced SOD1 Misfolding: Implications for Non-Amyloid Protein Aggregation in Familial ALS. *J. Mol. Biol.* **2012**, *421*, 631−652.
(24) Rodriguez, J. A.; Shaw, B. F.; Durazo, A.; Sohn, S. H.; Doucette, P. A.; Nersissian, A. M.; Faull, K. F.; Eggers, D. K.; Tiwari, A.; Hayward, L. J. Destabilization of Apoprotein is Insufficient to Explain Cu, Zn-Superoxide Dismutase Linked ALS Pathogenesis. *Proc. Natl. Acad. Sci. U.S.A.* **2005**, *102*, 10516−10521.
(25) Vassall, K. A.; Stubbs, H. R.; Primmer, H. A.; Tong, M. S.; Sullivan, S. M.; Sobering, R.; Srinivasan, S.; Briere, L.-A. K.; Dunn, S. D.; Colón, W.; Meiering, E. M. Decreased Stability and Increased Formation of Soluble Aggregates by Immature Superoxide Dismutase Do Not Account for Disease Severity in ALS. *Proc. Natl. Acad. Sci. U.S.A.* **2011**, *108*, 2210−2215.
(26) Nordlund, A.; Oliveberg, M. Folding of Cu/Zn Superoxide Dismutase Suggests Structural Hotspots for Gain of Neurotoxic Function in ALS: Parallels to Precursors in Amyloid Disease. *Proc. Natl. Acad. Sci. U.S.A.* **2006**, *103*, 10218−10223.
(27) Teilum, K.; Smith, M. H.; Schulz, E.; Christensen, L. C.; Solomentsev, G.; Oliveberg, M.; Akke, M. Transient Structural Distortion of Metal-Free Cu/Zn Superoxide Dismutase Triggers Aberrant Oligomerization. *Proc. Natl. Acad. Sci. U.S.A.* **2009**, *106*, 18273−18278.
(28) Lang, L.; Kurnik, M.; Danielsson, J.; Oliveberg, M. Fibrillation Precursor of Superoxide Dismutase 1 Revealed by Gradual Tuning of the Protein-Folding Equilibrium. *Proc. Natl. Acad. Sci. U.S.A.* **2012**, *109*, 17868−17873.
(29) Shen, J.; Subramaniam, S.; Wong, C. F.; McCammon, J. A. Superoxide Dismutase: Fluctuations in the Structure and Solvation of the Active Site Channel Studied by Molecular Dynamics Simulation. *Biopolymers* **1989**, *28*, 2085−2096.
(30) Chillemi, G.; Falconi, M.; Amadei, A.; Zimatore, G.; Desideri, A.; Di Nola, A. The Essential Dynamics of Cu, Zn Superoxide Dismutase: Suggestion of Intersubunit Communication. *Biophys. J.* **1997**, *73*, 1007−1018.
(31) Wade, R. C.; Gabdoulline, R. R.; Lüdemann, S. K.; Lounnas, V. Electrostatic Steering and Ionic Tethering in Enzyme-Ligand Binding: Insights from Simulations. *Proc. Natl. Acad. Sci. U.S.A.* **1998**, *95*, 5942−5949.
(32) Falconi, M.; Stroppolo, M. E.; Cioni, P.; Strambini, G.; Sergi, A.; Ferrario, M.; Desideri, A. Dynamics-Function Correlation in Cu, Zn Superoxide Dismutase: A Spectroscopic and Molecular Dynamics Simulation Study. *Biophys. J.* **2001**, *80*, 2556−2567.
(33) Khare, S. D.; Dokholyan, N. V. Common Dynamical Signatures of Familial Amyotrophic Lateral Sclerosis-Associated Structurally Diverse Cu, Zn Superoxide Dismutase Mutants. *Proc. Natl. Acad. Sci. U.S.A.* **2006**, *103*, 3147−3152.
(34) Strange, R. W.; Yong, C. W.; Smith, W.; Hasnain, S. S. Molecular Dynamics Using Atomic-Resolution Structure Reveal Structural Fluctuations That May Lead to Polymerization of Human Cu-Zn Superoxide Dismutase. *Proc. Natl. Acad. Sci. U.S.A.* **2007**, *104*, 10040−10044.
(35) Schmidlin, T.; Kennedy, B. K.; Daggett, V. Structural Changes to Monomeric CuZn Superoxide Dismutase Caused by the Familial Amyotrophic Lateral Sclerosis-Associated Mutation A4V. *Biophys. J.* **2009**, *97*, 1709−1718.
(36) Ding, F.; Dokholyan, N. V. Dynamical Roles of Metal Ions and the Disulfide Bond in Cu, Zn Superoxide Dismutase Folding and Aggregation. *Proc. Natl. Acad. Sci. U.S.A.* **2008**, *105*, 19696−19701.
(37) Proctor, E. A.; Ding, F.; Dokholyan, N. V. Structural and Thermodynamic Effects of Post-Translational Modifications in Mutant and Wild Type Cu, Zn Superoxide Dismutase. *J. Mol. Biol.* **2011**, *408*, 555−567.
(38) Ding, F.; Furukawa, Y.; Nukina, N.; Dokholyan, N. V. Local Unfolding of Cu, Zn Superoxide Dismutase Monomer Determines the Morphology of Fibrillar Aggregates. *J. Mol. Biol.* **2012**, *421*, 548−560.
(39) Das, S.; Plotkin, S. S. Mechanical Probes of SOD1 Predict Systematic Trends in Metal and Dimer Affinity of ALS-Associated Mutants. *J. Mol. Biol.* **2013**, *425*, 850−874.
(40) Das, S.; Plotkin, S. S. SOD1 Exhibits Allosteric Frustration to Facilitate Metal Binding Affinity. *Proc. Natl. Acad. Sci. U.S.A.* **2013**, *110*, 3871−3876.

(41) Harder, T.; Borg, M.; Bottaro, S.; Boomsma, W.; Olsson, S.; Ferkinghoff-Borg, J.; Hamelryck, T. An Efficient Null Model for Conformational Fluctuations in Proteins. *Structure* **2012**, *20*, 1028−1039.
(42) Irbäck, A.; Mitternacht, S.; Mohanty, S. An Effective All-Atom Potential for Proteins. *PMC Biophys.* **2009**, *2*, 2.
(43) Irbäck, A.; Mitternacht, S. Thermal Versus Mechanical Unfolding of Ubiquitin. *Proteins* **2006**, *65*, 759−766.
(44) Mitternacht, S.; Luccioli, S.; Torcini, A.; Imparato, A.; Irbäck, A. Changing the Mechanical Unfolding Pathway of FnIII-10 by Tuning the Pulling Strength. *Biophys. J.* **2009**, *96*, 429−441.
(45) Irbäck, A.; Mitternacht, S. Spontaneous β-Barrel Formation: An All-Atom Monte Carlo Study of Aβ_{16-22} Oligomerization. *Proteins* **2008**, *71*, 207−214.
(46) Li, D.; Mohanty, S.; Irbäck, A.; Huo, S. Formation and Growth of Oligomers: A Monte Carlo Study of an Amyloid Tau Fragment. *PLoS Comput. Biol.* **2008**, *4*, e1000238.
(47) Mitternacht, S.; Staneva, I.; Härd, T.; Irbäck, A. Monte Carlo Study of the Formation and Conformational Properties of Dimers of Aβ42 Variants. *J. Mol. Biol.* **2011**, *410*, 357−367.
(48) Tiana, G.; Sutto, L.; Broglia, R. A. Use of the Metropolis Algorithm to Simulate the Dynamics of Protein Chains. *Physica A* **2007**, *380*, 241−249.
(49) Vitalis, A.; Pappu, R. V. Methods for Monte Carlo Simulations of Biomacromolecules. *Annu. Rep. Comput. Chem.* **2009**, *5*, 49−76.
(50) Favrin, G.; Irbäck, A.; Sjunnesson, F. Monte Carlo Update for Chain Molecules: Biased Gaussian Steps in Torsional Space. *J. Chem. Phys.* **2001**, *114*, 8154−8158.
(51) Swendsen, R. H.; Wang, J. S. Replica Monte Carlo Simulation of Spin Glasses. *Phys. Rev. Lett.* **1986**, *57*, 2607−2609.
(52) Irbäck, A.; Mohanty, S. PROFASI: A Monte Carlo Simulation Package for Protein Folding and Aggregation. *J. Comput. Chem.* **2006**, *27*, 1548−1555.
(53) Strange, R. W.; Antonyuk, S.; Hough, M. A.; Doucette, P. A.; Rodriguez, J. A.; Hart, P. J.; Hayward, L. J.; Valentine, J. S.; Hasnain, S. S. The Structure of Holo and Metal-Deficient Wild-Type Human Cu, Zn Superoxide Dismutase and Its Relevance to Familial Amyotrophic Lateral Sclerosis. *J. Mol. Biol.* **2003**, *328*, 877−891.
(54) Chikenji, G.; Fujitsuka, Y.; Takada, S. Protein Folding Mechanisms and Energy Landscape of Src SH3 domain Studied by a Structure Prediction Toolbox. *Chem. Phys.* **2004**, *307*, 157−162.
(55) Frishman, D.; Argos, P. Knowledge-Based Protein Secondary Structure Assignment. *Proteins* **1995**, *23*, 566−579.
(56) DeLano, W. L. *The PyMOL Molecular Graphics System*; DeLano Scientific: San Carlos, CA, 2002.
(57) Stathopulos, P. B.; Rumfeldt, J. A. O.; Karbassi, F.; Siddall, C. A.; Lepock, J. R.; Meiering, E. M. Calorimetric Analysis of Thermodynamic Stability and Aggregation for Apo and Holo Amyotrophic Lateral Sclerosis-Associated Gly-93 Mutants of Superoxide Dismutase. *J. Biol. Chem.* **2006**, *281*, 6184−6193.
(58) Furukawa, Y.; Kaneko, K.; Yamanaka, K.; Nukina, N. Mutation-dependent polymorphism of Cu,Zn-Superoxide Dismutase Aggregates in the Familial Form of Amyotrophic Lateral Sclerosis. *J. Biol. Chem.* **2010**, *285*, 22221−22231.
(59) Trovato, A.; Seno, F.; Tosatto, S. C. E. The PASTA Server for Protein Aggregation Prediction. *Protein Eng. Des. Sel.* **2007**, *20*, 521−523.
(60) Banci, L.; Bertini, I.; Cramaro, F.; Del Conte, R.; Viezzoli, M. S. Solution Structure of Apo Cu,Zn Superoxide Dismutase: Role of Metal Ions in Protein Folding. *Biochemistry* **2003**, *42*, 9543−9553.
(61) Maurer-Stroh, S.; Debulpaep, M.; Kuemmerer, N.; Lopez de la Paz, M.; Martins, I. C.; Reumers, J.; Morris, K. L.; Copland, A.; Serpell, L.; Serrano, L.; Schymkowitz, J. W. H.; Rousseau, F. Exploring the Sequence Determinants of Amyloid Structure Using Position-Specific Scoring Matrices. *Nat. Methods* **2010**, *7*, 237−242.
(62) Oliveberg, M. Waltz, an Exciting New Move in Amyloid Prediction. *Nat. Methods* **2010**, *7*, 187−188.